Focused on Multiaxial Fatigue

Prediction of fatigue crack initiation under biaxial loading

J.V. Sahadi, D. Nowell, R.J.H. Paynter

University of University of Oxford, Department of Engineering Science, Parks Road, Oxford, OX1 3PJ, UK.
joao.sahadicavalheiro@eng.ox.ac.uk, david.nowell@eng.ox.ac.uk, robert.paynter@eng.ox.ac.uk

ABSTRACT. This investigation revisits biaxial fatigue experiments carried out with the nickel-based superalloy termed Waspaloy. Recently, yield criteria extended to multiaxial fatigue and stress based approaches were analysed and their performance to correlate the biaxial test data was evaluated. It was concluded that despite their reliable results, the parameters did not properly represent the physical behaviour of the material. In this context, an extension of this study was executed considering the strain based critical plane approaches proposed by Fatemi-Socie (FS) and Smith-Watson-Topper (SWT). The first parameter presented overly conservative predictions with large scatter of results. In contrast, more accurate predictions were obtained with the SWT parameter.

KEYWORDS. Biaxial fatigue; Fatigue Life; Waspaloy; Critical Plane Approach.

OPEN ACCESS

INTRODUCTION

Advances in material testing equipment and techniques during the past 40 years enabled the development of more realistic multiaxial fatigue tests by applying loads representative of service life, at different temperature settings (room, low or elevated temperatures), test frequencies and load phase shift. Among the most used techniques, cruciform specimens and thin-walled tubular specimens have been broadly used for fatigue testing under biaxial stress states [1]. Yet tension-torsion specimens pose limitations when it comes to probing the entire principal stress plane, σ_1 vs σ_2, and only 2 of its 4 quadrants can be investigated. Nevertheless, with different techniques, such as internally pressurized tubular specimens, it is possible to access more of the principal stress plane.

The combination of cruciform specimens and axial-torsional specimens, internally pressurized, allow the investigation of almost the entire principal stress plane. However, for cruciform specimens the assessment of biaxial compression region is commonly challenging due to testing machine limitations. In the literature, examples of fatigue life investigation using tubular specimens are available in [2–4]. Cruciform specimens and biaxial test rigs allow the investigation of a broad range of biaxiality. However, specimens are expensive and testing is complex. Work on biaxial testing with cruciform specimens can be found in [5–7].

Recent work at Oxford on biaxial fatigue testing and total life prediction using multiaxial fatigue criteria has been presented at the Eleventh International Conference on Multiaxial Fatigue and Fracture and published on the special issue of the conference [8]. The present paper presents further developments on the investigation of multiaxial fatigue criteria and their predictions for the biaxial test results presented at [8]

MATERIAL AND EXPERIMENTAL WORK

Our earlier work on multiaxial fatigue has presented biaxial tests employed for characterizing the fatigue behaviour of Waspaloy [8], a nickel-based superalloy widely used in aero-engines. Although the tests previously presented were performed at room temperature, this material presents elevated creep resistance, high fatigue strength, low thermal expansion coefficient and high thermal conductivity; essential characteristics to sustain the extreme mechanical and thermal loads which aero-engine disks are subject to. In terms of its mechanical properties, this material has an elastic Poisson's ratio of $\nu_e = 0.284$ and Young's modulus of 213GPa.

Load controlled tests were carried out at a load ratio of $R = 0.05$ and $0.5Hz$ frequency using a biaxial servo-hydraulic rig, developed and built at the University of Oxford. Fig. 1(a) presents the rig, which consists of two independent frames carrying hydraulic actuators such that the perpendicular load vectors meet at the centre of the specimen. The vertical load path has a fixed clamp at the top and an actuator at the bottom capable of providing up to 350kN. The horizontal load path has two actuators, providing up to 100kN each. The two frames are connected to each other through a set of springs, which allows vertical movement of the horizontal actuators according to the deformations of the specimen.

Fig. 1 (b) illustrates the cruciform specimen with reduced thickness gauge section at the centre. The centre portion (excluding the gauge section) was shot peened to increase the fatigue strength of the external edges between the arms and hence to inhibit failure away from the gauge section. Strain gauge rosettes were mounted on both front and back face of the gauge section and at the narrow point of the arms. The outputs from these were recorded, together with the applied loads, to determine a calibration of the specimen.
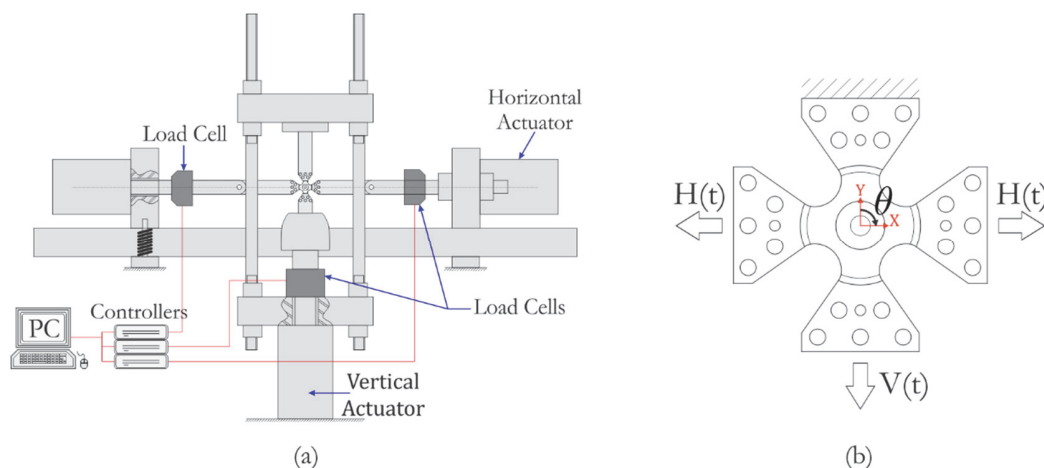

Figure 1: (a) Biaxial test rig. (b) Cruciform specimen, applied loads and definition of θ, positive clockwise.

Load Combinations

The original load conditions were set to have the same maximum principal stress in each case, varying the other in-plane principal stress. As the gauge section is only 2mm thick and 15mm across, the assumption is made that the local behaviour is equivalent to plane stress conditions, i.e. that the stress in the through thickness direction is zero. The following combinations were investigated:

−   Equal biaxial tension (EB): Equal load applied to each arm ($\sigma_1 = \sigma_2$);
−   Pure shear (PS): Stresses on the two axes are equal and opposite ($\sigma_1 = -\sigma_2$);
−   Single Actuator (Uniaxial Load – UL): Load applied on one axis only;
−   Uniaxial Stress (US): Both axes are used to create an uniaxial equivalent stress state at the gauge section ($\sigma_2 = 0$);
−   Minimum von Mises (Mv): The combination of loads that gives the minimum von Mises equivalent stress (octahedral shear stress) at the gauge section.

Experimental Results

Tab. 1 summarizes the results obtained after testing 11 specimens. As presented in more detail at [8], the initial tests compared different biaxialities at the same $\sigma_{1,peak}$ but different $\sigma_{2,peak}$ for each test. Following tests for pure shear and uniaxial

stress cases were run at lower peak stresses. It was observed that in most cases yielding occurred during the first cycle, but no "reversed yielding" took place when load was removed. Hence subsequent load cycles at the same load level did not cause additional plastic deformation despite the material being loaded close to the elastic limit on each cycle. Such observation is very important as it set the ground for the multiaxial criteria candidates for fatigue life prediction.

Exp. No.	Load case	Peak load [kN]		Norm. Peak Strain		Norm. Peak Stress			Biaxiality Ratio			Cycles
		Horizontal	Vertical	ε_x	ε_y	σ_x	σ_y	σ_{vM}	Load	Strain	Stress	
CX01	Single actuator	117	0	1.31	−0.71	1.21	−0.36	1.43	0	−0.54	−0.30	87,765
CX02	Equi-biaxial	170	170	0.88	0.88	1.23	1.23	1.23	1	1	1	65,426
CX03	Equi-biaxial	170	170	0.88	0.88	1.23	1.23	1.23	1	1	1	57,884
CX04	Single actuator	117	0	1.31	−0.71	1.21	−0.36	1.43	0	−0.54	−0.30	97,560
CX05	Pure shear	90	−90	1.56	−1.56	1.21	−1.21	2.1	−1.00	−1.00	−1.00	25,789
CX06	Pure shear, low ε	51	−51	0.88	−0.88	0.69	−0.69	1.19	−1.00	−1.00	−1.00	510,000 (Runout)
CX07	Uniaxial Eq.	128.5	38.5	1.21	−0.34	1.21	0	1.21	0.3	−0.28	0	154,396
CX08	Min von Mises	147.8	102.8	1.04	0.26	1.21	0.61	1.05	0.7	0.25	0.5	107,004
CX09	Uniaxial Eq., low ε	93.6	28.1	0.88	−0.25	0.88	0	0.88	−1.00	−0.28	0	658,164
CX10	Pure shear, low σ	65.5	−65.5	1.13	−1.13	0.88	−0.88	1.53	−1.00	−1.00	−1.00	236,935
CX11	Pure shear	90	−90	1.56	−1.56	1.21	−1.21	2.1	−1.00	−1.00	−1.00	21,684

Table 1: Experimental tests parameters and results.

ANALYSIS

Stress-based criteria

An introductory analysis of the test data was achieved by considering extensions of yield theories to multiaxial fatigue and stress based criteria. The formulations of von Mises, elastic strain energy equivalent stress, Crossland [9], Findley [10]and Matake [11] were investigated. Among them, the energy parameter and Crossland's invariant based approach gave the best predictions.

The elastic strain energy density is the sum of the products of strain and stress (divided by 2). In the case of plane stress and no shear, a uniaxial stress with equivalent strain energy to a biaxial stress state is formulated as:

$$\sigma_{Ue} = \sqrt{\sigma_1^2 + \sigma_2^2 - 2\upsilon\left(\sigma_1^2\sigma_2^2\right)} \qquad (1)$$

where υ represents the Poisson's ratio. Fig. 2 (a) presents the correlation between this parameter normalized and the test data in cycles to failure. The stress-life curve was obtained using Basquin's relation (power relationship) and using the equivalent stress presented in Eq. (1). The criterion presented good results with a coefficient of correlation, r², of 0.868. Among all the test cases, the pure shear low stress case was the furthest to the trend line.

In sequence, some of the most widely used stress based criteria were investigated. The stress invariant based criterion proposed by Crossland [9] considers the amplitude of the second invariant of the deviatoric stress tensor, J_{2a} (which corresponds to the amplitude of von Mises equivalent stress) and the maximum value of the first invariant of Cauchy's

stress tensor, i.e. the maximum hydrostatic stress, $\sigma_{h,max}$. This last term accounts for the mean stress effect. The criterion is given as:

$$\sqrt{J_{2a}} + \kappa \sigma_{h,max} \leq \lambda \ , \tag{2}$$

where κ and λ are material constants determined under fully reversed tension (σ_{-1}) and torsion (τ_{-1}) tests with smooth specimens respectively:

$$\kappa = 3\left(\frac{\tau_{-1}}{\sigma_{-1}}\right) - \sqrt{3} \ ; \quad \lambda = \tau_{-1} \ , \tag{3}$$

Fig. 2 (b) presents the fatigue life predictions obtained with this formulation, considering various fatigue thresholds, i.e. a test case below a line is predicted to have a longer fatigue life than the threshold of the line. On the other hand, a point above it represents a test case with shorter life. The light grey shade area corresponds to the calibrated region (tension-torsion), and is delimited by the uniaxial tension dashed lines. The darker grey shade area is delimited by the equi-biaxial line. The dashed black lines connect test cases with the same $\sigma_{1,peak}$, in order to illustrate the biaxiality effect when $\sigma_{2,peak}$ is changed.

It was concluded that in general the model presents good correlation with experimental data both within and outside the calibration region (tension-torsion region). Non-conservative predictions were obtained for negative values of $\sigma_{2,peak}$ (pure shear and uniaxial load cases -- CX01, CX04, CX05 and CX10). In contrast, as $\sigma_{2,peak}$ increases towards higher positive values, the criterion becomes proportionally more conservative (min von Mises and equi-biaxial – CX08, CX02 and CX03).
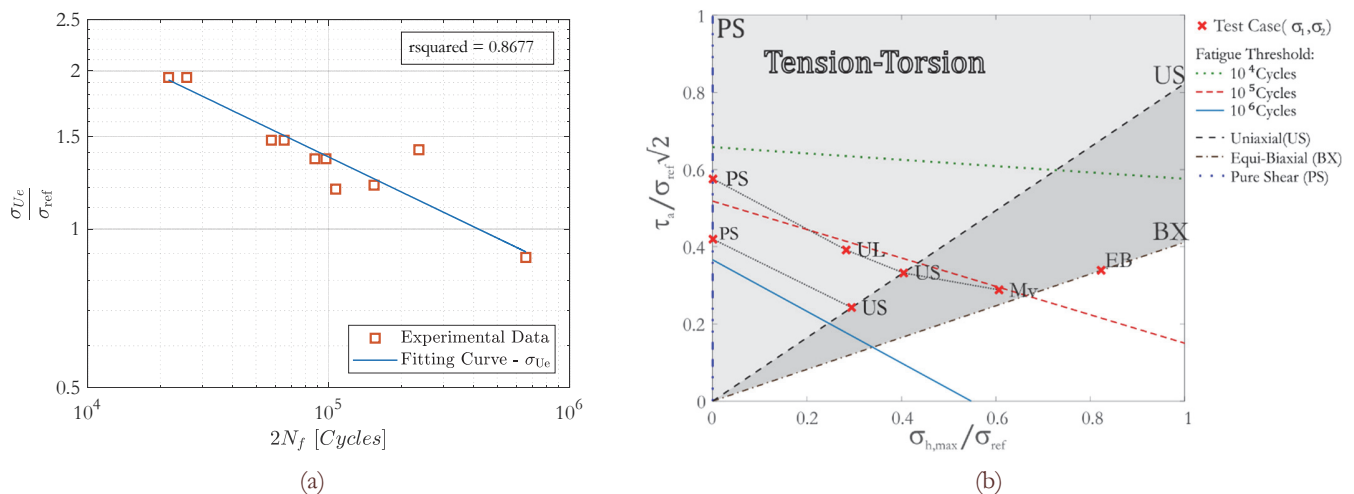

Figure 2: (a) Fatigue life predictions with elastic strain energy density. (b) according to Crossland's criterion.

Strain-based criteria

Despite the satisfactory results obtained with the stress-based criteria, it was concluded in the previous investigation that the concept of additive parameters does not properly represent the physical behaviour of materials. In this context, a further investigation was performed considering strain based critical plane approaches. This class of strain-based methods is based on the search for critical planes (one or more) where a particular damage parameter reaches its maximum magnitude. This methodology has gained great attention over the past 40 years as it mathematically describes the physical phenomenon and is capable of predicting damage and also the crack orientation (for ductile materials cracks typically nucleate along slip planes, where the maximum shear stress occurs [12,13]). In this sense, among the most widely used criteria the Fatemi-Socie [14] and Smith-Watson-Topper [15] parameters were evaluated.

Based on the work of Brown and Miller [13], Fatemi and Socie [14] arrived at the conclusion that tensile normal stress in the maximum shear stress plane accelerates crack growth by separating the crack surfaces and consequently reducing frictional forces. The following damage model may be interpreted as the cyclic shear strain modified by the normal stress to include the crack closure effects described.

$$\frac{\Delta\gamma_{\max}}{2}\left(1+\kappa\frac{\sigma_{n,\max}}{\sigma'_{\text{yield}}}\right)=\frac{\tau'_f}{G}\left(2N_f\right)^{b\gamma}+\gamma'_f\left(2N_f\right)^{c\gamma} \tag{4}$$

where $\Delta\gamma_{\max}/2$ is the maximum shear strain amplitude and $\sigma_{n,\max}$ is the maximum normal stress on the plane where $\Delta\gamma_{\max}/2$ occurs. The material parameter κ represents the influence of the normal stress, $\sigma_{n,\max}$. In addition, σ'_{yield} represents the cyclic yield strength of the material and is included to make the maximum normal stress component dimensionless and proportional to the shear strain. τ'_f and b_γ are the shear fatigue strength coefficient and exponent respectively. γ'_f and c_γ are the shear fatigue ductility coefficient and exponent respectively.

The material parameter κ is given as:

$$\kappa=\left(\frac{\frac{\tau'_f}{G}\left(2N_f\right)^{b\gamma}+\gamma'_f\left(2N_f\right)^{c\gamma}}{\left(1+\nu_e\right)\frac{\sigma'_f}{E}\left(2N_f\right)^{b}+\left(1+\nu_p\right)\varepsilon'_f\left(2N_f\right)^{c}}-1\right)\frac{\sigma'_{\text{yield}}}{\sigma'_f\left(2N_f\right)^{b}} \tag{5}$$

Fig. 3(a) illustrates the evolution of the Fatemi-Socie (FS) parameter presented in Eq. (4) and (5), the shear strain amplitude ($\Delta\gamma/2$) and the normal stress (σ_n) as a function of the angle θ, varying from 0 to 180°. Considering the angle orientation presented in Fig. 1 (b), for all the tests analysed in here the critical planes predicted by this parameter are orientated at 45° and 135° from the y-axis.
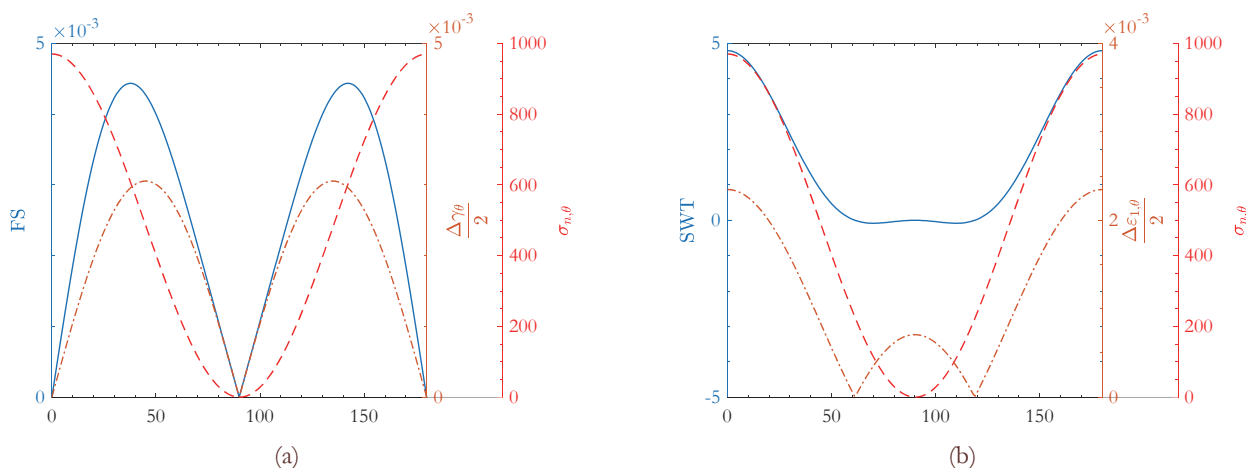

Figure 3: (a) Evolution of Fatemi-Socie parameter (FS), $\Delta\gamma/2$ and σ_n as a function of angle θ for proportional loading. (b) Evolution of Smith-Watson-Topper parameter (SWT), $\Delta\varepsilon_1/2$ and σ_n as a function of angle θ for proportional loading.

Smith-Watson-Topper

The second damage parameter considered was proposed by Smith et al. [59], SWT, and was proposed for predicting fatigue life under uniaxial tension-compression conditions. The parameter was originally defined as,

$$\sigma_{n,\max}\varepsilon_a=\frac{\sigma'^2_f}{E}\left(2N_f\right)^{2b}+\sigma'_f\varepsilon'_f\left(2N_f\right)^{b+c}, \tag{6}$$

where σ'_f and b are the axial fatigue strength coefficient and exponent respectively. Similarly ε'_f and c represents the axial fatigue ductility coefficient and exponent.

This parameter was modified for proportional and non-proportional multiaxial loading conditions of materials that fail predominantly by crack growth on planes of maximum tensile strain or stress, according to crack Mode I. In these materials, cracks nucleate in shear, but early life is controlled by crack growth on planes perpendicular to the maximum principal stress and strain. Socie [16] proposed a modification to the SWT parameter in order to take into account only stresses and strains occurring in the critical plane. This became the most well-known form of the parameter and is mathematically represented by

$$\sigma_{n,max} \frac{\Delta \varepsilon_1}{2} = \frac{\sigma_f'^2}{E} \left(2N_f\right)^{2b} + \sigma_f' \varepsilon_f' \left(2N_f\right)^{b+c}, \tag{7}$$

where, $\Delta\varepsilon_1/2$ represents the maximum normal stress, and accordingly $\sigma_{n,max}$ is calculated on the plane where $\Delta\varepsilon_1/2$ occurs. Fig. 3 (b) illustrates the evolution of this parameter with respect to θ, along with $\Delta\varepsilon_n/2$ and σ_n. The critical planes predicted with this formulation are orientated at 0 and 180º from the y-axis, as oriented in Fig. 1 (b).

Fig. 5 presents the fully reversed normal strain-life curve used to calibrate the models. Since no shear strain-life curves were available at the time of this analysis, the additional material parameters needed for the Fatemi-Socie criterion were estimated based on the relationships presented in Tab. 2. Moreover, the results and material parameters presented in the work of Lopez-Crespo et al [17] were used as a benchmark for verifying the implementation of both parameters.

Parameter	Axial	Shear
Fatigue Strength Coefficient	σ_f'	$\tau_f' \approx \sigma_f' / \sqrt{3}$
Fatigue Strength Exponent	b	$b_\gamma \approx b$
Fatigue Ductility Coefficient	ε_f'	$\gamma_f' \approx \sqrt{3}\varepsilon_f'$
Fatigue Ductility Exponent	c	$c_\gamma \approx c$
Modulus	E	$G = \dfrac{E}{2(1+\nu)}$

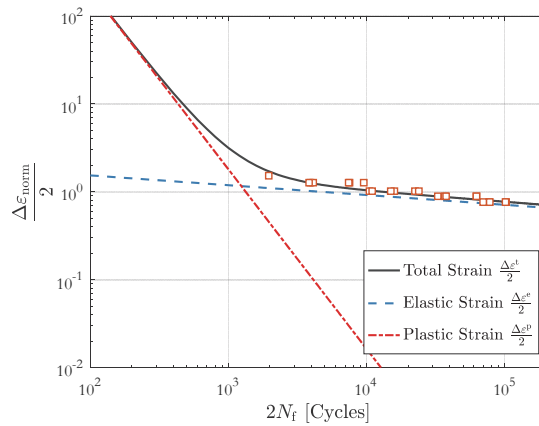Table 2: Correlation between material fatigue parameters.

Figure 4: Strain-life curve used for model calibration.

Fatigue Life Prediction

After calibrating both models, their performances were assessed using the biaxial test data presented in Tab. (1) (for this analysis, the runout (CX06) was not considered). Fatigue lives were calculated using Eqs. (4), (5) and (7) at the material plane where each of the parameters (FS and SWT) reached their maximum. The results were plotted against the experimental fatigue lives in Fig. 5 and summarized in Tab. (3). The solid black line in the plot represents perfect correlation between predicted and experimental life. In contrast, predictions lying above this line represent non-conservative predictions, and data points below the line represents conservative predictions. Further, the dashed lines represent the bounds of twice and half of the fatigue life.

It is observed that the Fatemi-Socie parameter presented conservative predictions, with all its results in the safe area of the plot. As $\sigma_{2,peak}$ magnitude decreases towards the uniaxial loading and uniaxial stress conditions(CX1, CX4 and CX07), the prediction error increased proportionally. The farthest point to the solid black line corresponds to CX07 under uniaxial stress state condition. Nevertheless, the parameter presented good correlation with the equi-biaxial loading cases (CX02 and

CX03), with predictions within the bound of half of fatigue life. The inferior performance of the parameter could be attributed to the estimation of shear strain-life coefficients and exponents based on the available normal strain-life curve. Dissimilarly, predictions with the SWT parameter are in better correlation with the experimental data, with less scatter. Most of the fatigue life predictions lie within the two bound lines. The data points closely aligned with the solid black line represent the pure shear (CX05, CX10, CX11), the uniaxial equivalent (CX09) and the minimum von Mises (CX08) cases. The conditions slightly out of the area delimited by the two dashed black line correspond to single actuator and equi-biaxial loading conditions, which presented the largest error. Analogously, the superior performance of this second parameter could be related to its calibration, independent of the shear strain-life curve parameters.
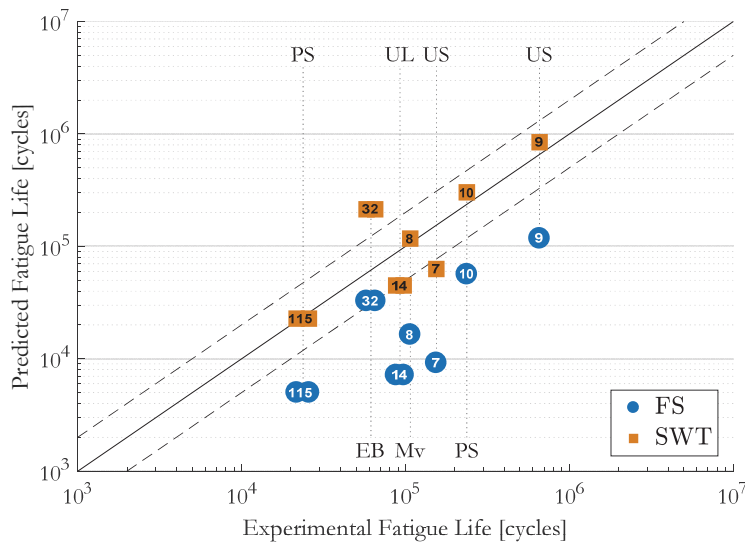

Figure 5: Fatigue life predicted with Fatemi-Socie and Smith-Watson-Topper parameters.

Exp. №	Load case	Fatemi-Socie		Smith-Watson-Topper	
		Critical Planes $[\theta]$	Predicted Life	Critical Planes	Predicted Life
CX01	Single actuator	45° and 135°	7,170	0° and 180°	44,910
CX02	Equi-biaxial	45° and 135°	32,680	0° and 180°	213,570
CX03	Equi-biaxial	45° and 135°	32,680	0° and 180°	213,570
CX04	Single actuator	45° and 135°	7,170	0° and 180°	44,910
CX05	Pure shear	45° and 135°	5,010	0° and 180°	22,790
CX07	Uniaxial Eq.	45° and 135°	9,200	0° and 180°	62,880
CX08	Min von Mises	45° and 135°	16,430	0° and 180°	117,380
CX09	Uniaxial Eq., low ε	45° and 135°	117,910	0° and 180°	842,890
CX10	Pure shear, low σ	45° and 135°	56,460	0° and 180°	302,600
CX11	Pure shear	45° and 135°	5,010	0° and 180°	22,790

Table 3: Fatigue life predictions with Fatemi-Socie and Smith-Watson Topper parameters.

CONCLUSIONS

Further investigation of the biaxial fatigue behaviour of Waspaloy concluded that even more advanced formulations, as the strain based critical plane approaches assessed here, give poor correlations for the equi-biaxial loading cases. The lack of torsional fatigue data, and the estimation of some of these parameter for the implementation of the Fatemi-Socie formulation, resulted in poor correlation with most test cases. Furthermore, the FS parameter presented an overly conservative behaviour with great scatter of results. In contrast, the SWT parameter presented better correlation with the biaxial fatigue data. Predictions obtained with it lied mostly within or near the bounds of twice and half of the fatigue life. Finally, regarding the evaluation of critical planes, the FS parameter predicted failure nucleating on planes at 45º and 135º of the vertical axis, and the SWT predicted failures on planes at 0º and 180º.

ACKNOWLEDGMENTS

REFERENCES

[1] Bonnand, V., et al. Investigation of multiaxial fatigue in the context of turboengine disc applications. International Journal of Fatigue, 33(8) (2011) 1006-1016.

[2] Kalluri, S., Bonacuse, P. J., In-phase and out-of-phase axial-torsional fatigue behavior of haynes 188 superalloy at 760 C. Advances in multiaxial fatigue. ASTM International, (1993).

[3] Found, M. S., Upul, S. F., Miller, K. J., Requirements of a new multiaxial fatigue testing facility. Multiaxial fatigue. ASTM International, (1985).

[4] Andrews, J. M. H., Ellison, E. G., A testing rig for cycling at high biaxial strains. Journal of Strain Analysis, 8(3) (1973) 168-175.

[5] Makinde, A., Thibodeau, L., Neale, K. W., Development of an apparatus for biaxial testing using cruciform specimens. Experimental mechanics, 32(2) (1992) 138-144.

[6] Boehler, J. P., Demmerle, S., Koss, S., A new direct biaxial testing machine for anisotropic materials. Experimental mechanics, 34(1) (1994) 1-9.

[7] Hannon, A., Tiernan, P., A review of planar biaxial tensile test systems for sheet metal. Journal of materials processing technology, 198(1) (2008) 1-13.

[8] Sahadi, J. V., et al., Comparison of multiaxial fatigue parameters using biaxial tests of Waspaloy. International Journal of Fatigue (2017).

[9] Crossland, B., Effect of large hydrostatic pressures on the torsional fatigue strength of an alloy steel. Proc. Int. Conf. on Fatigue of Metals. Vol. 138. Institution of Mechanical Engineers London, (1956).

[10] Findley, W. N., A theory for the effect of mean stress on fatigue of metals under combined torsion and axial load or bending. No. 6. Engineering Materials Research Laboratory, Division of Engineering, Brown University, (1958).

[11] Matake, T., An explanation on fatigue limit under combined stress. Bulletin of JSME 20.141 (1977) 257-263.

[12] Socie, D. F., Marquis, G. B., Multiaxial Fatigue. Warrendale, Pa: Society of Automotive Engineers, (2000).

[13] Brown, M. W., Miller, K. J., A theory for fatigue failure under multiaxial stress-strain conditions. Proceedings of the Institution of Mechanical Engineers, 187(1) (1973) 745-755.

[14] Kurath, P., Multiaxial fatigue life predictions under the influence of mean-stresses. Urbana, 51 (1988) 61801.

[15] Smith, K. N., Topper, T. H., Watson, P., A stress-strain function for the fatigue of metals(Stress-strain function for metal fatigue including mean stress effect), Journal of materials, 5 (1970) 767-778.

[16] Socie, D. F., Multiaxial fatigue damage models. Transactions of the ASME. Journal of Engineering Materials and Technology, 109(4) (1987) 293-298.

[17] Lopez-Crespo, P., et al. Study of crack orientation and fatigue life prediction in biaxial fatigue with critical plane models. Engineering Fracture Mechanics, 136 (2015) 115-130.